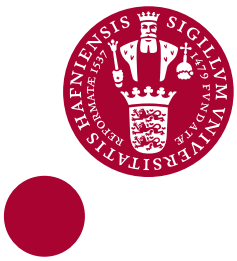

Structural determinants underlying permeant discrimination of the Cx43 hemichannel

Nielsen, Brian Skriver; Zonta, Francesco; Farkas, Thomas; Litman, Thomas; Nielsen, Morten Schak; Macaulay, Nanna

Published in:
Journal of Biological Chemistry

DOI:
10.1074/jbc.RA119.007732

Publication date:
2019

Document version
Publisher's PDF, also known as Version of record

Structural determinants underlying permeant discrimination of the Cx43 hemichannel

Received for publication, January 25, 2019, and in revised form, September 24, 2019 Published, Papers in Press, September 25, 2019, DOI 10.1074/jbc.RA119.007732

Brian Skriver Nielsen[‡], **Francesco Zonta**[§], **Thomas Farkas**[¶], **Thomas Litman**[¶], **Morten Schak Nielsen**[‖], and **Nanna MacAulay**[‡1]

From the Departments of [‡]*Neuroscience,* [¶]*Immunology and Microbiology, and* [‖]*Biomedical Sciences, Faculty of Health and Medical Sciences, University of Copenhagen, 2200 Copenhagen, Denmark and the* [§]*Shanghai Institute for Advanced Immunochemical Studies, ShanghaiTech University, Shanghai 201210, China*

Edited by Roger J. Colbran

Connexin (Cx) gap junction channels comprise two hemichannels in neighboring cells, and their permeability is well-described, but permeabilities of the single Cx hemichannel remain largely unresolved. Moreover, determination of isoform-specific Cx hemichannel permeability is challenging because of concurrent expression of other channels with similar permeability profiles and inhibitor sensitivities. The mammalian Cx hemichannels Cx30 and Cx43 are gated by extracellular divalent cations, removal of which promotes fluorescent dye uptake in both channels but atomic ion conductance only through Cx30. To determine the molecular determinants of this difference, here we employed chimeras and mutagenesis of predicted pore-lining residues in Cx43. We expressed the mutated channels in *Xenopus laevis* oocytes to avoid background activity of alternative channels. Oocytes expressing a Cx43 hemichannel chimera containing the N terminus or the first extracellular loop from Cx30 displayed ethidium uptake and, unlike WT Cx43, ion conduction, an observation further supported by molecular dynamics simulations. Additional C-terminal truncation of the chimeric Cx43 hemichannel elicited an even greater ion conductance with a magnitude closer to that of Cx30. The inhibitory profile for the connexin hemichannels depended on the permeant, with conventional connexin hemichannel inhibitors having a higher potency toward the ion conductance pathway than toward fluorescent dye uptake. Our results demonstrate a permeant-dependent, isoform-specific inhibition of connexin hemichannels. They further reveal that the outer segments of the pore-lining region, including the N terminus and the first extracellular loop, together with the C terminus preclude ion conductance of the open Cx43 hemichannel.

Direct intercellular communication can be maintained by gap junction channels, which allow exchange of atomic ions as well as a variety of biological molecules, such as second messengers and metabolites, between the cell interiors (1). A gap junction is formed when two connexons/hemichannels assemble between two neighboring cells, and each of these pore-forming hemichannels consists of six connexins (Cx)[2] (2). 21 different human connexin isoforms are identified and numbered according to their molecular weight (3). The connexin isoform composition is decisive for the permeability profile of gap junction channels, which exhibit great variations in their cation *versus* anion selectivity, single-channel conductance, and permeability to different fluorescent dyes and biological molecules (1, 4, 5). In recent years, it has become evident that connexins not only have the ability to form functional channels coupling two neighboring cells, but also may be active as unopposed hemichannels that, if open, act as transport routes between the intra- and extracellular space (6). The (patho)physiological roles of connexin hemichannels are under investigation, but assignment of exact implications of each channel isoform in various physiological processes is complicated by the overlapping permeability and inhibitory profiles between the various isoforms of connexin hemichannels and other large-pore membrane channels in complex cell systems (7–11). It therefore, to a large extent, remains unresolved which classes of molecules permeate a given open hemichannel. Do these transmembrane channels, when open, act essentially as half a gap junction with a permeation profile identical to its gap junctional counterpart? Or do they display pore selectivity distinct for their hemichannel configuration?

The pore-lining region of a connexon originates from the N terminus (folding into the pore area (12)), the transmembrane segment 1 (TM1), and the first extracellular loop (E1) (12–16) (see Fig. 1). Molecular studies have indicated that upon docking with a hemichannel counterpart on a neighboring cell to form a gap junction, the channel alters its conformation, and distinct sets of amino acid side chains face the interior of the pore-lining region of the channel in the hemichannel *versus* the gap junction configuration (17, 18). With all three segments of the predicted pore-lining region potentially being involved in pore selectivity, this structural rearrangement may alter the channel permeability between a given connexin-based gap junction and its hemichannel and thus provide these two channel configurations with distinct permeability profiles.

This work was supported by the Faculty of Health and Medical Sciences, University of Copenhagen (to B. S. N. and N. M.) and by National Natural Science Foundation of China Grant 31770776 (to F. Z.). The authors declare that they have no conflicts of interest with the contents of this article.

[1] To whom correspondence should be addressed: University of Copenhagen, Blegdamsvej 3, 2200 Copenhagen N, Denmark. Tel.: 45-35327566; E-mail: macaulay@sund.ku.dk.

[2] The abbreviations used are: Cx, connexin(s); Px, pannexin; TM1, transmembrane region 1; NT, N terminus; E1, extracellular loop 1; DCFS, divalent cation-free solution; FFA, flufenamic acid; CBX, carbenoxelone; ddH2O, double-distilled H_2O; ANOVA, analysis of variance.

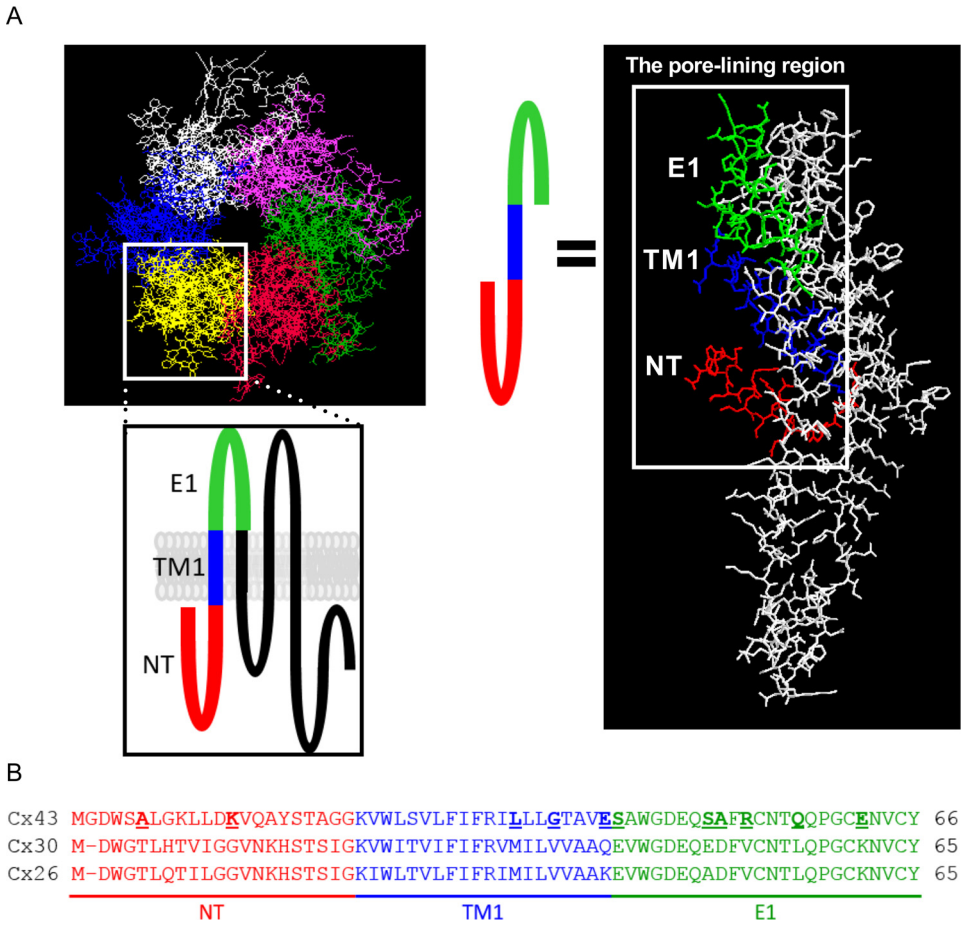

Figure 1. Homology model of Cx43 and alignment of the predicted pore-lining region of Cx43, Cx30 and Cx26. *A*, image depicting a homology model of a Cx43 gap junctional channel (amino acids 1–244), based on the Cx26 gap junction structure. The predicted pore-lining region is *highlighted* and *colored* in the typology drawing as well as in the structure of the Cx43 monomer. *B*, alignment of the predicted pore-lining region of Cx43, Cx30, and Cx26. The residues of Cx43 selected for mutagenesis are *underscored* and *highlighted* in *boldface type*.

Fluorescent dyes are routinely used to quantify gap junction and hemichannel activity (19–24). The rationale behind the use of this technique is that the dye permeability may mirror the permeability of biological molecules of the same size or smaller than that of the fluorescent dye used (20, 25–27) and could as such be employed as a readout of general channel activity. Gap junctions are permeable to fluorescent dyes, biological molecules, and atomic ions, although each isoform displays subtle preferences for some types of molecules over others (1, 4, 5, 28). It has, however, in recent years become evident that this non-selective gap junction permeability may not translate to its hemichannel activity: Hemichannels appear to be able to distinguish between different permeants in a manner indicating that fluorescent dye uptake is not proportional to the permeability of smaller biological molecules and atomic ions (11, 29, 30). Hemichannels composed of Cx26, Cx30, or Cx43 readily open upon removal of divalent cations, whether expressed in *Xenopus* oocytes or mammalian cells (6, 11, 20–22, 29–40). Once open, these channels display distinct selectivity to fluorescent dye *versus* atomic ions (current) with Cx26 promoting membrane currents and little, if any, ethidium uptake, Cx30 promoting membrane current and ethidium uptake, and Cx43 promoting ethidium uptake but no membrane current (at physiological membrane potentials) (11, 29, 30). To resolve the molecular determinants underlying the ability of Cx43 hemichannels to discriminate between atomic ions and a fluorescent dye in its permeation pathway, we expressed different connexin isoforms, as well as chimeras and point mutants thereof, in isolation in *Xenopus* oocytes. The biophysical characterization, aided by molecular dynamics simulations, of these constructs pointed to the outer sections of the predicted pore-lining region of the hemichannel configuration, namely the N terminus and the extracellular loop 1, as the molecular determinants preventing Cx43 hemichannel-mediated membrane conductance.

Results

Single amino acid substitutions in the pore region of the Cx43 hemichannel do not confer ion conductance to Cx43

To determine the molecular determinants underlying the ability of Cx43 to discriminate between atomic ions and ethidium, we created a homology model of Cx43 based on the high-resolution structure of Cx26, presumably in its gap junctional configuration (12) (Fig. 1*A*). With this model, Cx43 pore-lining residues could be identified and aligned with the equivalent region in Cx26 and Cx30 (see Fig. 1*B*). Those amino acids that differed between Cx43 and the ion-conducting Cx26 and Cx30 isoforms were subsequently replaced by site-directed

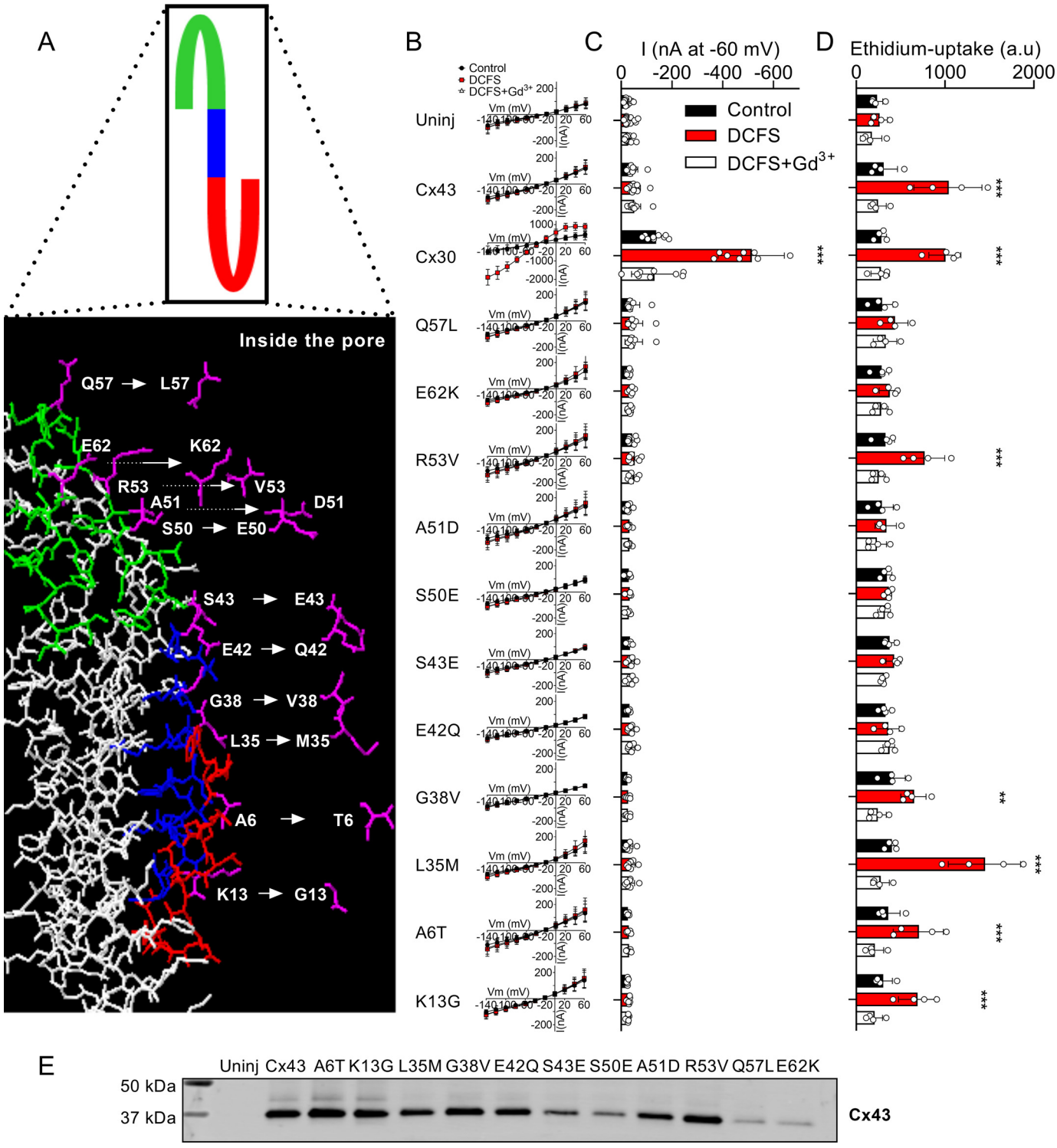

Figure 2. Mutagenesis of select pore-lining residues does not alter Cx43 hemichannel ion conductance. *A*, illustrates the predicted pore-lining region of a Cx43 monomer with the select predicted pore-lining residues that were mutated individually to the aligned amino acid in Cx30, marked in *pink*. *B*, *I/V* curves from uninjected and Cx30-, Cx43-, and Cx43 mutant-expressing oocytes ($n = 17$, $n = 9$, $n = 11$, and $n \geq 7$ for the mutations, respectively). *C*, summarized membrane currents obtained at −60 mV. *D*, ethidium uptake in uninjected and Cx30-, Cx43-, and Cx43 mutant-expressing oocytes (all $n = 4$). *E*, Western blotting showing oocyte surface expression of Cx43 or the 11 Cx43-mutated constructs. Data in *I/V* curves and in the bar graphs are presented as mean ± S.D. (*error bars*). Statistical significance of DCFS-induced hemichannel activity within each group was tested using repeated-measures two-way ANOVA (current, interaction: $F_{(26,208)} = 46.9$, $p < 0.001$; construct: $F_{(13,104)} = 68.3$, $p < 0.001$; test solution: $F_{(2,208)} = 55.0$, $p < 0.001$; and Eth, interaction: $F_{(26,84)} = 13.2$, $p < 0.001$; construct: $F_{(13,42)} = 4.2$, $p < 0.001$; test solution: $F_{(2,84)} = 184.7$, $p < 0.001$) with Dunnett's post hoc test (against control). **, $p < 0.01$; ***, $p < 0.001$.

mutagenesis with the amino acid found at the equivalent site in Cx30 (illustrated in Fig. 2*A*). To reveal if single amino acid chains could be decisive for hemichannel-mediated conductance, the membrane current and ethidium uptake of uninjected and Cx-expressing *Xenopus* oocytes were determined in control solution (frog Ringer's solution, containing 1 mM Ca^{2+} and

1 mM Mg^{2+}), in divalent cation-free solution (DCFS), and in DCFS containing the connexin hemichannel inhibitor gadolinium (Gd^{3+}). Cx30 hemichannel-mediated membrane current has a low Ca^{2+} sensitivity, and the 1 mM Ca^{2+} in the standard frog Ringer does not suffice to fully block the hemichannel activity, hence the elevated control current in oocytes expressing this isoform (30, 35). Of the 11 mutated Cx43 constructs individually expressed in oocytes, none displayed the DCFS-induced membrane conductance observed in Cx30-expressing oocytes (Fig. 2, *B* and *C*) and thus behaved similarly to uninjected and WT Cx43–expressing oocytes. A subset of the mutant Cx43 hemichannels (A6T, K13G, L35M, G38V, and R53V) displayed DCFS-mediated ethidium uptake comparable with the Cx30- and Cx43-expressing oocytes, whereas the remainder of the mutant constructs (and the uninjected oocytes) displayed no DCFS-induced ethidium uptake (Fig. 2*D*). Verification of plasma membrane expression of the mutated Cx43 hemichannels was conducted with surface biotinylation of oocytes expressing these constructs followed by Western blotting (Fig. 2*E*). Our results indicate that no single amino acid in the Cx43 hemichannel pore acts as a determinant of hemichannel conductance.

Incorporation of the outer pore-lining regions from Cx30 into Cx43 promotes hemichannel ion conductance

Because single amino acid substitutions in the pore-lining region of Cx43 failed to confer ion conductivity to Cx43 hemichannels, we created a chimeric Cx43, in which the entire predicted pore-lining region (consisting of the N terminus, the first transmembrane segment, and the first extracellular loop (12)) of Cx43 was exchanged with that of the ion-conducting Cx30 ($Cx43^{30}$; illustrated in Fig. 3*A*). Surface biotinylation of oocytes expressing the chimeric $Cx43^{30}$ showed proper expression and translocation of the protein to the plasma membrane (Fig. 3*A*, *bottom right corner*). Despite abundant $Cx43^{30}$ membrane expression, $Cx43^{30}$-expressing oocytes displayed no DCFS-induced membrane conductance or ethidium uptake (Fig. 3, *B–D*). These data illustrate that incorporation of the entire predicted pore-lining region of Cx30 into Cx43 produced a nonfunctional hemichannel. We therefore, instead, exchanged single sections of the predicted pore-lining region in Cx43 with that of Cx30: the N terminus ($Cx43^{30NT}$), the transmembrane domain 1 ($Cx43^{30TM1}$), or the extracellular loop 1 ($Cx43^{30E1}$), illustrated in Fig. 4*A*. Expression and translocation of these chimeras to the oocyte plasma membrane were verified by surface biotinylation and Western blotting (Fig. 4*A*, *bottom right corner*). Replacement of the N terminus ($Cx43^{30NT}$) or the extracellular loop ($Cx43^{30E1}$) with that of Cx30 yielded small, but detectable, DCFS-activated conductance in oocytes expressing these constructs (Fig. 4, *B* and *C*). The membrane conductance was paralleled by DCFS-induced ethidium uptake similar to that of the Cx30- and Cx43-expressing oocytes (Fig. 4*D*). Oocytes expressing the chimeric version of Cx43 with the first transmembrane domain replaced with that from Cx30 ($Cx43^{30TM1}$) did not demonstrate DCFS-induced membrane conductance or ethidium uptake (Fig. 4, *B–D*). These results suggest that the outer sections of the predicted pore-lining region of Cx43, the N terminus and the extracellular loop 1, are crucial structures for the ability of Cx43 to selectively discriminate between atomic ions and ethidium in its permeation pathway.

The extracellular loop 1 and both termini contribute to the atomic ion impermeability of the Cx43 hemichannel

The C terminus of Cx43 has previously been implicated in the gating of atomic ion permeation in Cx43 hemichannels (30). To determine the C-terminal involvement in the ability of Cx43 to discriminate between ethidium and atomic ions, we created a chimeric Cx43 combining all permissive regions: C-terminal truncation (Met-237) combined with a replacement of the N terminus and the first extracellular loop with that of Cx30 ($Cx43M257^{30NT\text{-}E1}$), illustrated in Fig. 5*A*. Oocytes expressing this chimeric Cx43 hemichannel displayed robust DCFS-activated membrane conductance (Fig. 5, *B* and *C*) and parallel ethidium uptake (Fig. 5*D*). These data indicate that it is not the TM1 section of the predicted pore-lining region of Cx43, but rather the part of the pore consisting of the N terminus and the extracellular loop 1, that, together with the C terminus, provide Cx43 with its isoform-specific permeability filter.

Molecular dynamics simulations support ion permeability in WT Cx30 and in the $Cx43^{30NT\text{-}E1}$ chimeric hemichannel

To elucidate the differences between the two hemichannels at the molecular level, we performed molecular dynamics simulations of Cx30 and Cx43 hemichannels in a realistic environment including membrane, water, and ions mimicking the physiological ionic strength (Fig. 6, *A* and *B*). For these simulations, we created homology models of Cx30 (based on the available structure of Cx26 (12), which is similar to Cx30) and of Cx43 (based on the available structure of Cx46/Cx50 (41), which is similar to Cx43). In addition, the Cx43 chimera with the N terminus and the first extracellular loop replaced with that of Cx30 ($Cx43^{30NT\text{-}E1}$) was also modeled, as well as two selected point mutations in the E1 part of the pore-lining region (Cx43.S43E and Cx43.S50E). As the C terminus of these proteins is very flexible, it cannot be modeled with any degree of fidelity and is therefore left out in all of the mentioned models. Ionic permeation pathways can be compared by analyzing the density profile of ions inside the hemichannel during the molecular dynamics trajectory (42). The K^+ density profile was remarkably higher in the part of the pore-lining region consisting of the E1 region bordering TM1 in Cx30 than in Cx43 (Fig. 6, *C* and *D*). These findings indicate that the Cx30 hemichannels appear to be more prone to recruit potassium ions near its extracellular vestibule, and thus facilitate potassium permeation, compared with Cx43 hemichannels. Moreover, in agreement with the experimental results, the substitution of the Cx30 E1 region and N terminus into the Cx43 hemichannel in our model ($Cx43^{30NT\text{-}E1}$) produces a K^+ density profile similar to that of Cx30 (Fig. 6*D*). One possible interpretation of these results is that the E1 loop in Cx30 is important to help in passing the major bottleneck that is located at the E1 region bordering TM1 (43) and favors the translocation of K^+ ions from the extracellular region to the cytoplasmic, or vice versa, depending on the applied external potential. The aspartic and glutamic

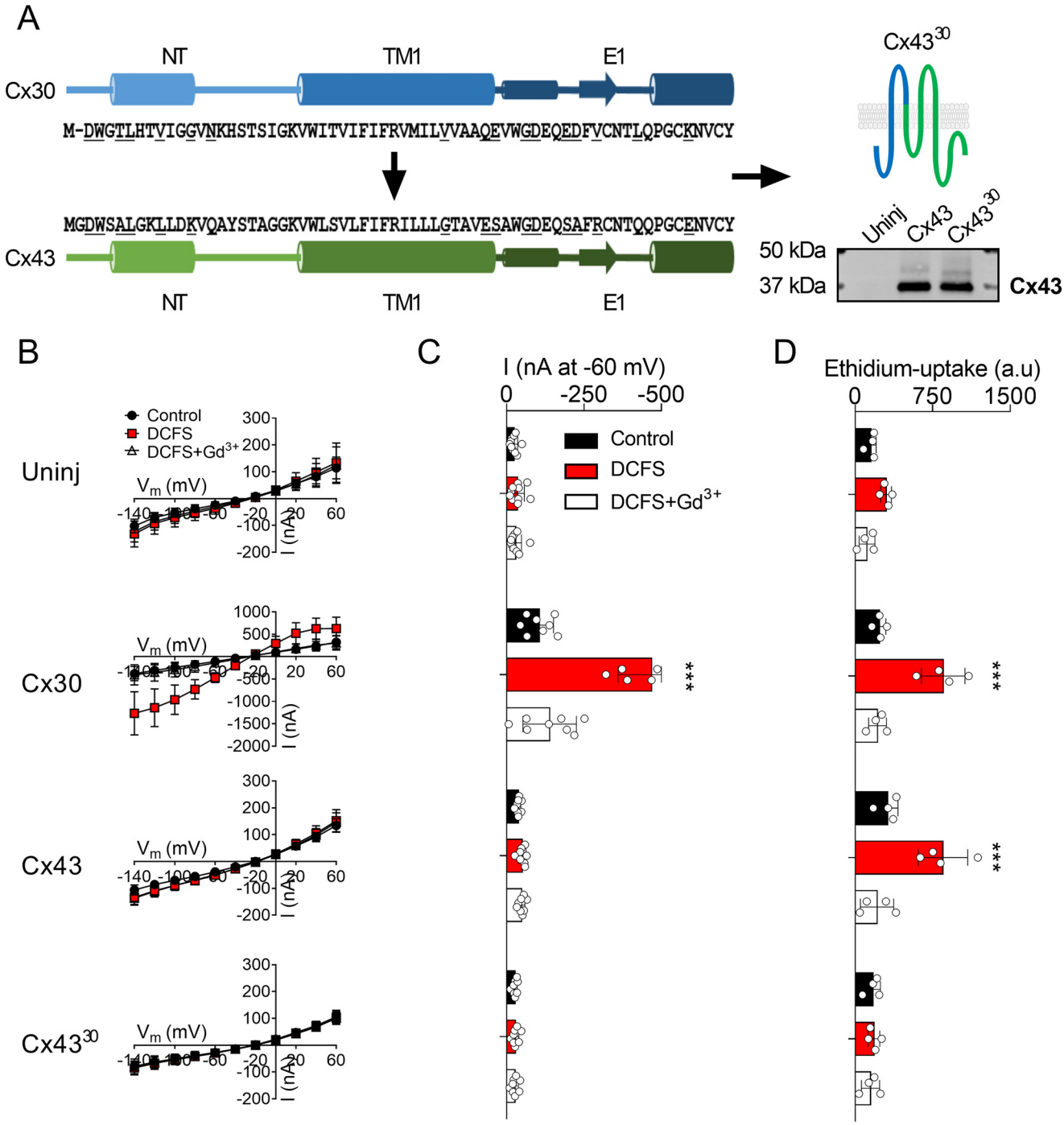

Figure 3. Cx43 chimera with the predicted pore-lining region of Cx30 display no ion conductance or ethidium uptake. *A*, alignment of the NT, TM1, and E1 of Cx30 and Cx43 with the predicted pore-lining residues underlined in the amino acid sequence as well as an illustration of the Cx43 chimera containing the predicted pore-lining region of Cx30. Western blotting of oocyte surface expression of Cx43 and Cx43^{30} is shown in the *bottom right corner*. *B*, *I*/V curves from uninjected and Cx30-, Cx43-, and Cx43^{30}-expressing oocytes ($n = 10$, $n = 8$, $n = 8$, and $n = 8$, respectively). *C*, summarized membrane currents obtained at −60 mV. *D*, ethidium uptake from uninjected and Cx30-, Cx43-, and Cx43^{30}-expressing oocytes (all $n = 4$). Data in *I*/V curves and in the bar graphs are presented as mean ± S.D. (*error bars*). Statistical significance of DCFS-induced hemichannel activity within every group was tested using repeated-measures two-way ANOVA (current, interaction: $F_{(8,74)} = 214.8$, $p < 0.001$; construct: $F_{(4,37)} = 54.1$, $p < 0.001$; test solution: $F_{(2,74)} = 254.4$, $p < 0.001$ and Eth, interaction: $F_{(6,24)} = 7.2$, $p < 0.001$; construct: $F_{(3,12)} = 30.0$, $p < 0.001$; test solution: $F_{(2,24)} = 38.5$ $p < 0.001$) with Dunnett's post hoc test (against control). ***, $p < 0.001$.

acids in this region appear critical to create a favorable environment for cations. Cx30 is richer in acidic side chains and thus favors the passage of such ions: in Cx30, Asp-50, Glu-49, and Glu-42 are exposed to the solvent, whereas Asp-46 is buried and forms a hydrogen bond with Gln-48 of the adjacent connexin (Fig. 6*E*). In Cx43, Glu-42 (which is homologous with Gln-41 of Cx30) is the only acidic residue in the pore-lining region, with Asp-47 and Gln-49 serving the same functions as the homologous Asp-46 and Gln-48 of Cx30 (Fig. 6, *E* and *F*). Nevertheless, single amino acid substitution of Ser-43 and Ser-50 alone is not sufficient to significantly modify the properties of Cx43 hemichannels, as shown in our experimental

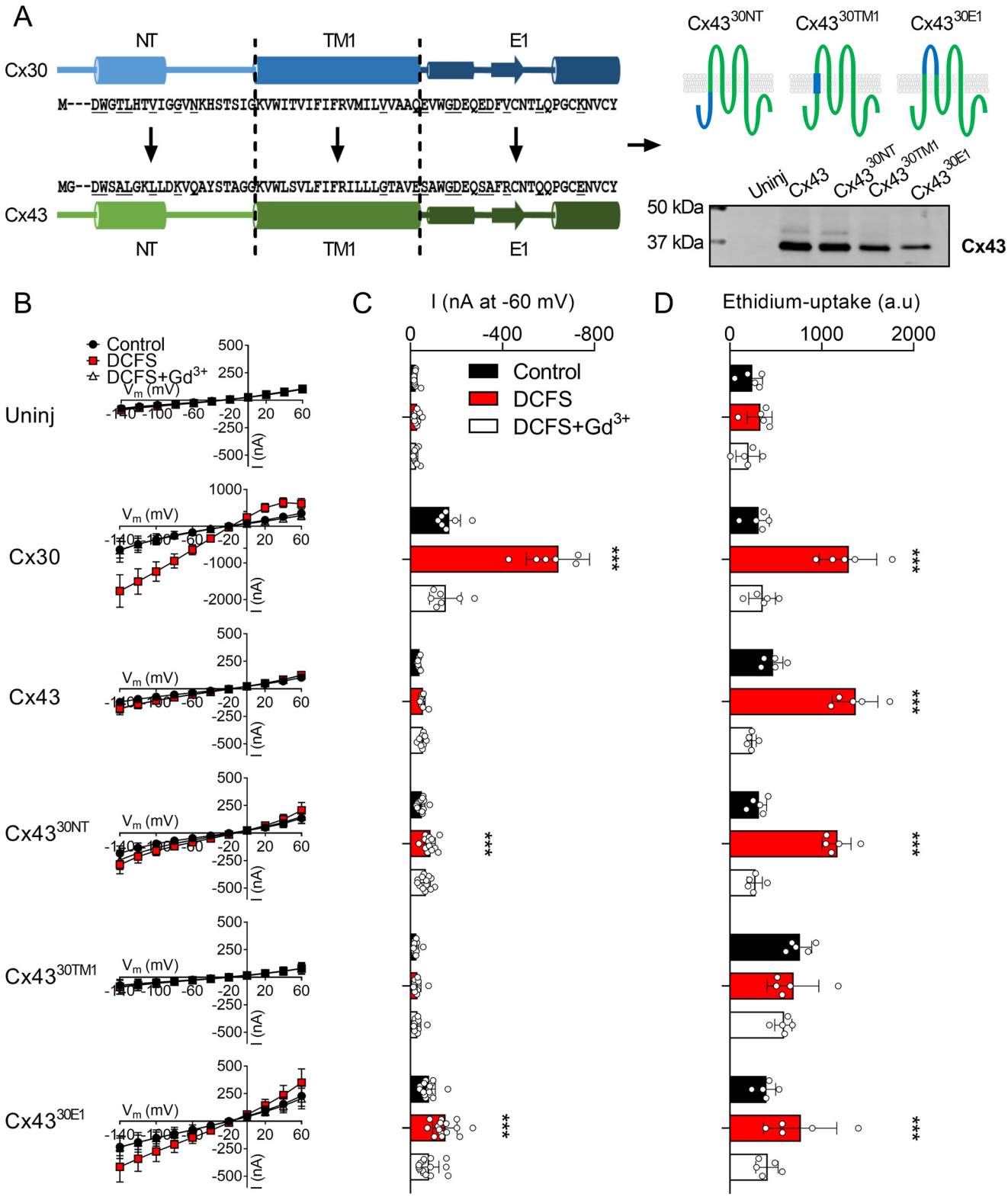

Figure 4. Cx43 chimeras containing the N terminus or the extracellular loop 1 of the Cx30 display DCFS-activated membrane currents. *A*, alignment of the NT, TM1, and E1 of Cx30 and Cx43 with the predicted pore-lining residues *underlined* in the amino acid sequence as well as an illustration of Cx43 chimeras containing the NT, TM1, or the E1 from Cx30. Western blotting of oocyte surface expression of Cx43, Cx43^{30NT}, Cx43^{30TM1}, and Cx43^{30E1} in the *bottom right corner*. *B*, summarized *I*/V curves from uninjected and Cx30-, Cx43-, Cx43^{30NT}-, Cx43^{30TM1}-, and Cx43^{30E1}-expressing oocytes ($n = 11$, $n = 7$, $n = 9$, $n = 13$, $n = 11$, and $n = 15$, respectively): summarized membrane currents obtained at −60 mV. *D*, ethidium uptake in uninjected and Cx30-, Cx43-, Cx43^{30NT}-, Cx43^{30TM1}-, and Cx43^{30E1}-expressing oocytes (all $n = 5$). Data in *I*/V curves and in the bar graphs are presented as mean ± S.D. (*error bars*). Statistical significance of DCFS-induced hemichannel activity within each group was tested using repeated-measures two-way ANOVA (current, interaction: $F_{(10,120)} = 137.5$, $p < 0.001$; construct: $F_{(5,60)} = 92.8$, $p < 0.001$; test solution: $F_{(2,120)} = 315.5$, $p < 0.001$ and Eth, interaction: $F_{(10,48)} = 20.3$, $p < 0.001$; construct: $F_{(5,24)} = 6.2$, $p < 0.001$; test solution: $F_{(2,48)} = 182.8$ $p < 0.001$) with Dunnett's post hoc test (against control). ***, $p < 0.001$.

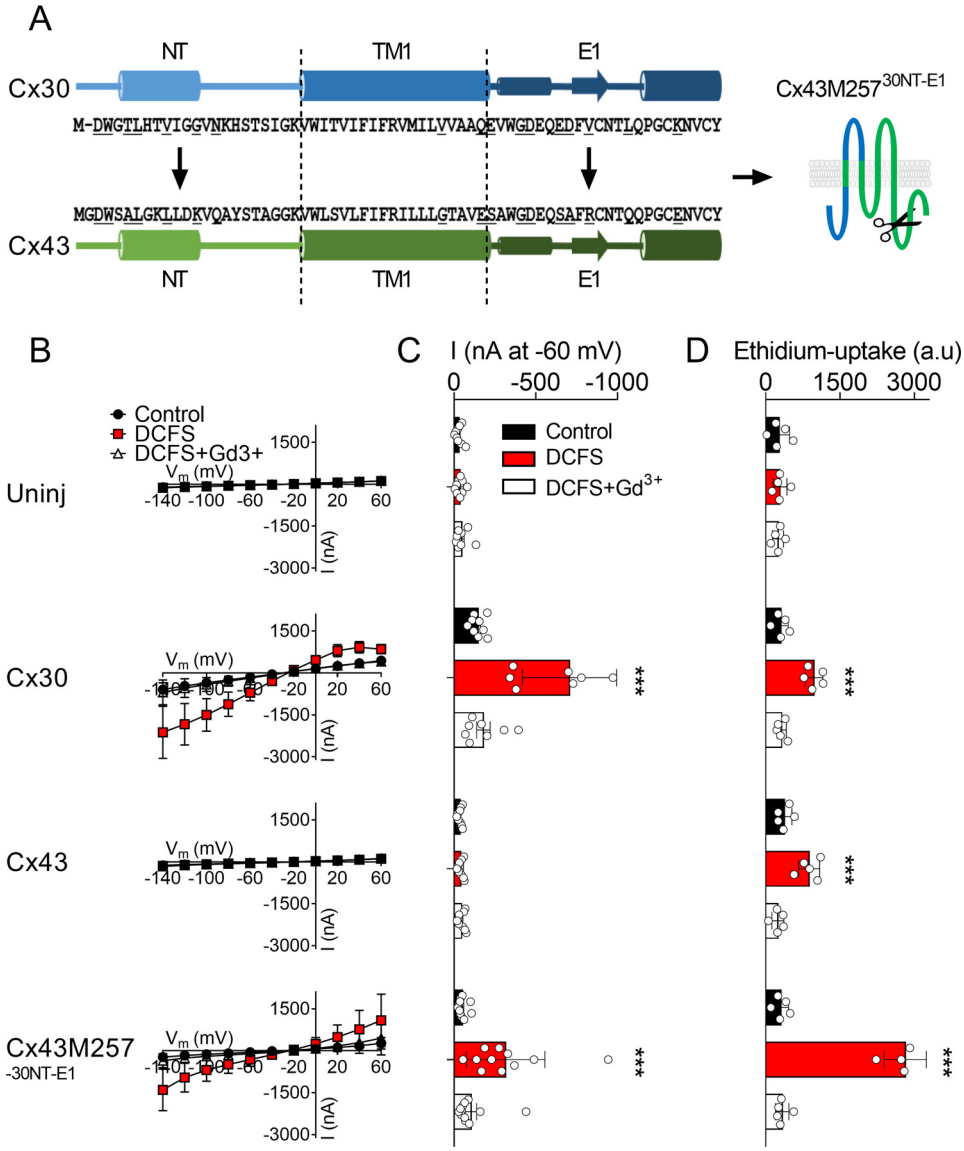

Figure 5. Combination of C-terminal truncation of Cx43 (Met-257) with the incorporation of both the N terminus and the first extracellular loop of Cx30 enhances the DCFS-activated membrane currents. *A*, alignment of the NT, TM1, and E1 of Cx30 and Cx43 with the predicted pore-lining residues *underlined* in the amino acid sequence as well as an illustration of the Cx43M257 chimera containing the NT and the E1 from Cx30. *B*, summarized *I*/*V* curves from uninjected and Cx30-, Cx43-, and Cx43M257$^{30NT-E1}$-expressing oocytes ($n = 9$, $n = 9$, $n = 9$, $n = 10$, and $n = 11$, respectively). *C*, summarized membrane currents obtained at −60 mV. *D*, ethidium uptake in uninjected and Cx30-, Cx43-, and Cx43M257$^{30NT-E1}$-expressing oocytes (all $n = 5$). Data in *I*/*V* curves and in the bar graphs are presented as mean ± S.D. (*error bars*). Statistical significance of DCFS-induced hemichannel activity within every group was tested using repeated measures two-way ANOVA (current, interaction: $F_{(6,64)} = 20.9$, $p < 0.001$; construct: $F_{(3,32)} = 16.5$, $p < 0.001$; test solution: $F_{(2,64)} = 51.5$, $p < 0.001$; and Eth, interaction: $F_{(6,32)} = 64.5$, $p < 0.001$; construct: $F_{(3,16)} = 43.3$, $p < 0.001$; test solution: $F_{(2,32)} = 194.6$, $p < 0.001$) with Dunnett's post hoc test (against control) when significant. ***, $p < 0.001$.

results. In agreement with this observation, ion density along the channel axis is not significantly different in the Cx43.S43E mutant when compared with its WT counterpart. On the other hand, we observe a peak in K^+ density in the proximity of Glu-50 in the Cx43.S50E mutant. These ions, however, remain localized around the position of the Glu-50 side chain and cannot penetrate deeper in the channel. The atomistic models, instead, appear insufficient to discriminate between the two hemichannels and the chimera at the level of the N terminus. It is possible that the N terminus is involved in gating mechanisms that are elicited in response to the external membrane potential. Such transition likely appears on a timescale much longer that those achievable with atomistic simulations (44).

Connexin hemichannels display permeant-dependent isoform-specific inhibition profiles

The specificity of the compounds used to block connexin hemichannels remains to be resolved, as does the ability of the commonly used inhibitors to target the different permeants, here in the form of ethidium uptake and membrane currents. A range of commonly used inhibitors in the Cx/Px field were tested for their ability to inhibit Cx26-, Cx30-, and Cx43-mediated hemichannel activity. The inhibitor profile of Cx30- and Cx43-expressing oocytes was tested for ethidium uptake (as we detect negligible ethidium uptake in Cx26-expressing oocytes (29)), and the inhibitor profile of Cx26- and Cx30-expressing oocytes was determined for ion conductance (as we are unable to detect ion conductance in Cx43-expressing oocytes (this

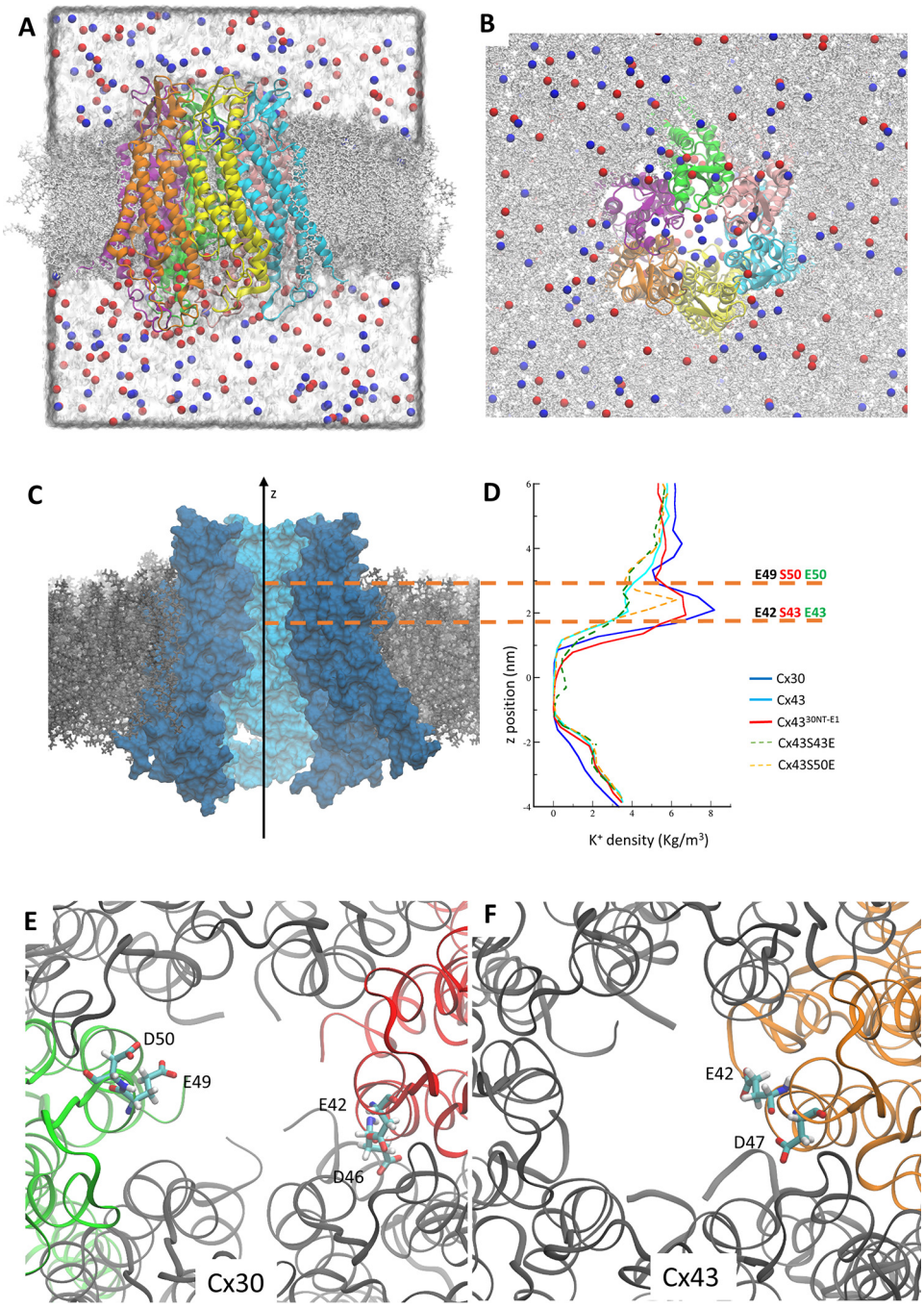

Figure 6. Molecular dynamics of Cx30, Cx43, and Cx43$^{30NT-E1}$ hemichannels. *A* and *B*, side (*A*) and extracellular (*B*) view of the Cx30 model. The hemichannel was inserted in a phospholipid bilayer, and simulations were performed in an explicit solvent environment. Each of the six connexins composing the hemichannel is represented with a *different color*. K^+ is *blue*, and Cl^- is *red*. In *A*, which represents a single snapshot of the simulation, it is possible to notice the accumulation of K^+ in the extracellular part of the channel. *C*, Cx30 hemichannel embedded in the phospholipid bilayer. The proteins are represented according to their predicted solvent-accessible surfaces. Two connexins are removed to show the internal part of the channel. *D*, the graphs show the K^+ density along the *z* axis of the different hemichannels during the molecular dynamics simulations. The *z* positions are centered on the midpoint of mass of each hemichannel, and the graphs are reported in register with the Cx30 hemichannel represented in *C*. The two *orange dotted lines* show the position of residues 42 and 49 in Cx30, which correspond to 43 and 50 for Cx43 and Cx43$^{30NT-E1}$. It is evident how K^+ accumulates in the extracellular vestibule of Cx30 and Cx43$^{30NT-E1}$, compared with Cx43. *E* and *F*, the position of acidic residues facing the pore in the E1 region for Cx30 (*E*) and Cx43 (*F*). For clarity, we report the position in one or two connexin polypeptides only.

study and 30). The inhibitor response of the uninjected oocytes was negligible, but it was deducted from the data to obtain the connexin-specific response. Flufenamic acid (FFA) conferred isoform-specific inhibition of the connexin hemichannel-mediated conductance (IC_{50} = 5.9 ± 0.9 μM (n = 9) for Cx26 and 27.4 ± 8.0 μM (n = 7) for Cx30) with no effect on the Cx30- and Cx43-mediated ethidium uptake (n = 5) (Fig. 7*A*). Lanthanum (La^{3+}) inhibited both conductance and dye permeability in the tested connexin hemichannels (Eth IC_{50} = 0.7 ± 0.2 μM (n = 4) for Cx30 and 0.8 ± 0.2 μM (n = 5) for Cx43; current IC_{50} = 2.2 ± 0.2 μM (n = 8) for Cx26 and 2.8 ± 0.2 μM (n = 10) for Cx30) with around 4 times higher potency toward ethidium

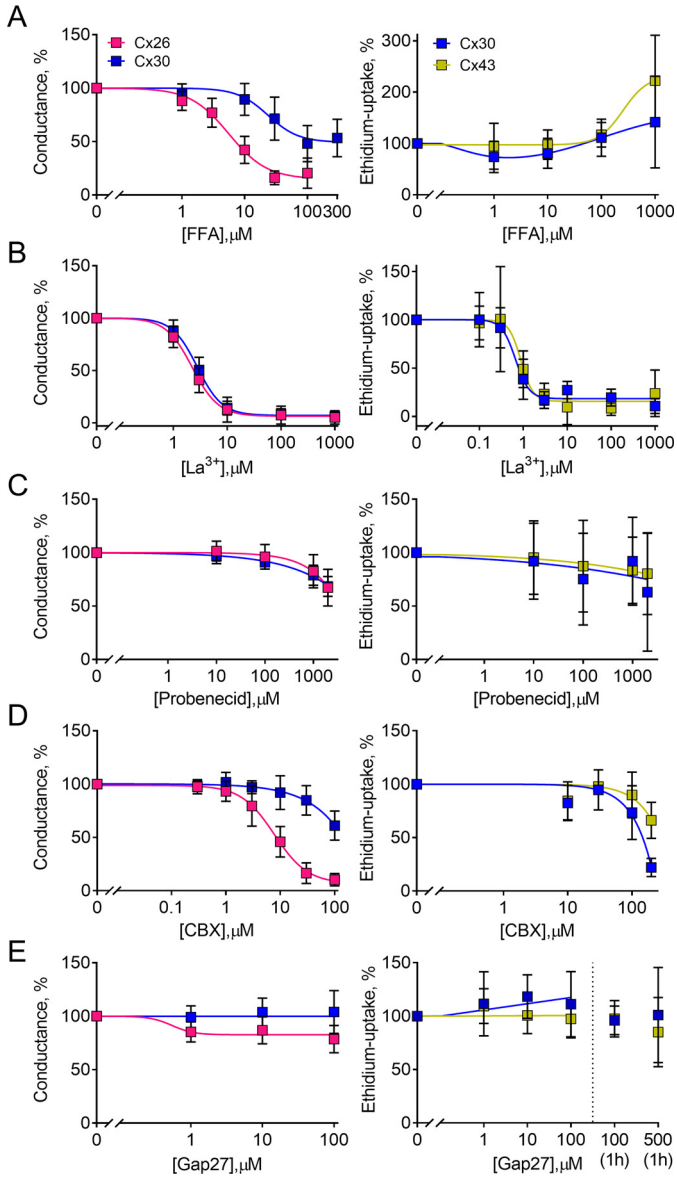

Figure 7. Permeant-dependent isoform-specific inhibition. *A–E, left panels*, Cx26- and Cx30-mediated currents were obtained in DCFS with the indicated inhibitor concentrations (n = 6–11). Membrane currents were recorded in DCFS from +60 to −140 mV in steps of 20 mV from a holding potential of −30 mV, and the currents recorded at −120 mV were used for the inhibitor sensitivity curves upon normalization to the current obtained in the absence of inhibitor or peptide. *A–E* (*right panels*), ethidium uptake was determined in Cx30- and Cx43-expressing oocytes after a 40-min exposure to DCFS with the drug concentrations indicated (n = 3–6). For gap27, an additional exposure time of 1 h (preincubated) was performed with 100 and 500 μM (n = 3). Uninjected oocyte background uptake was subtracted, and the hemichannel-mediated ethidium uptake was normalized to the control uptake in the absence of inhibitor. Data are presented as mean ± S.D. (*error bars*).

uptake than membrane conductance (Fig. 7*B*). The well-established pannexin 1 inhibitor probenecid had little, if any, effect on the Cx30- and Cx43-mediated ethidium uptake (n = 6), while exerting a slight inhibitory effect on connexin hemichannel-mediated conductance at high concentrations (n = 9) (Fig. 7*C*). Isoform-specific inhibitory potency was observed for carbenoxelone (CBX) on both ethidium uptake and ion conductance; Cx30-mediated ethidium uptake was more sensitive to CBX than that of Cx43 at the highest concentration tested (n = 3 of each), whereas the ion conductance mediated by Cx26 was more sensitive to CBX (IC_{50} = 8.2 ± 1.4 μM, n = 11) than the Cx30-mediated ion conductance (IC_{50} > 100 μM, n = 9) (Fig. 7*D*). Under the present conditions, the Cx43-specific mimetic peptide gap27 displayed no effect on the Cx30/43 hemichannel-mediated ethidium uptake (n = 4) or the Cx26/30-mediated hemichannel-mediated conductance (n = 6), not even with prolonged exposure to high concentrations (n = 3) (Fig. 7*E*). These results suggest that the inhibitory profiles of the tested connexin hemichannels depend on the nature of the permeant and that select blockers display isoform-specific inhibition.

Discussion

The present study identifies the outer sections of the predicted pore-lining region (the N terminus and the first extracellular loop) in conjunction with the C terminus of Cx43 as the protein regions of Cx43 that enable discrimination between atomic ions and ethidium in its hemichannel configuration.

It has generally been inferred that a connexin in its hemichannel configuration acts as a "half gap junction" and thus displays a permeability profile akin to that. Nonbiological fluorescent dyes are routinely used as a permeability proxy for ions or biological molecules based on dye size and charge in both gap junction and hemichannel research (20, 25–27). As an emerging indicator for the selectivity of Cx43 in its hemichannel configuration, a growing number of research groups have detected Cx43-mediated dye uptake at negative membrane potentials, at which DCFS-induced Cx43 hemichannel conductance is undetectable in mammalian cells (cell lines and primary cultures) as well as in *Xenopus* oocytes (11, 29, 30, 45–48). To reveal the structural determinants underlying the ability of Cx43 to preclude ion conductance in its open (ethidium-permeable) hemichannel configuration, we took advantage of a select set of connexin hemichannels with distinct permeation profiles (29, 30). These connexins, and mutant versions thereof, were individually expressed in *Xenopus laevis* oocytes, which allow biophysical channel characterization in an isolated setting devoid of the large background catalogue of similar candidate channels present in complex cell systems. As a potential pitfall to this strategy, connexin expression in any heterologous expression system may be affected by factors absent or present in cell types with native connexin expression, including phosphorylation state, interaction partners, membrane lipids, etc. However, the overlapping inhibitor profile, manners of activation, and permeation profiles of a range of large-pore channels expressed in complex cells simply prevent detailed biophysical characterization in these native settings. Whereas there has been some concern about the *X. laevis* expression system due its endogenous Cx38 expression (49, 50), predominantly based on a study of overexpression of Cx38 in oocytes (50), we have observed no functional difference between uninjected control oocytes and oocytes co-injected with siRNA targeting Cx38 (30), nor between our uninjected control oocytes and Cx38 siRNA-injected oocytes from other research groups (51, 52). We are therefore convinced that the reported functional readout represents hemichannel activity via the heterologously overexpressed connexin.

Molecular determinants of Cx43 permeation

To delineate the Cx43 molecular determinants that specifically allow it to discriminate against atomic ions in its hemichannel permeation pathway, we took advantage of Cx30, which displays robust DCFS-induced hemichannel conductance in addition to its ethidium permeability, whether expressed in mammalian cells or oocytes (29, 30, 32, 35, 40). While awaiting a high-resolution crystal structure of Cx30 or Cx43, we employed the 3.5 Å X-ray crystal structure of Cx26 (12) as an atomic model to predict the structure of Cx43. Whereas homology modeling is currently our most promising approach, one must bear in mind that a model of Cx43 hemichannels based on a Cx26 gap junction structure may well provide incomplete insight into the exact location of the pore-lining residues due to differences in protein arrangement and conformational organization. Nevertheless, due to the high sequence similarity in the transmembrane and extracellular region within the connexin family, it is believed that the overall structure and topology of the connexin protein are largely conserved within the protein family. Our SWISS-MODEL homology model of Cx43 together with sequence alignment of Cx30 and Cx43 revealed 11 pore-lining amino acid differences of particular interest (predominantly involving charged amino acids) between Cx30 and Cx43. None of the resulting 11 single mutations introduced in Cx43, to mimic the Cx30 hemichannel, displayed DCFS-induced hemichannel-mediated ion conductance, suggesting that no single pore-lining amino acid provides Cx43 with the ability to discriminate between atomic ions and ethidium. Of the 11 mutations, those six located in or near the extracellular loop abolished hemichannel-mediated ethidium uptake despite proper membrane localization. The lack of mutant hemichannel function suggests that this part of Cx43 is strictly organized and that mutations in this area may interrupt cysteine residue disulfide linkages important for structural integrity, and thus likely function, of the connexin hemichannels (53, 54). The predicted pore-lining part of the connexin hemichannels originates from three different segments of the channel: the N terminus, the TM1, and the E1 (Fig. 1) (12). Individual replacement of each of these three sections of the pore-lining region in Cx43 with those from Cx30 yielded two Cx43 hemichannel chimeras (one with the Cx30 N terminus ($Cx43^{30NT}$) and one with the Cx30 extracellular loop 1 ($Cx43^{30E1}$)) with the ability to mediate both ethidium uptake and membrane current. These observations thus demonstrate that the part of the pore residing in the membrane, the TM1, is not the predictor of Cx43 hemichannel-mediated membrane conductance. The modulatory role of these outer pore-lining Cx43 segments aligns well with their established role in gap junctional gating: The altered ion conductance property of the N-terminal chimera ($Cx43^{30NT}$) might be explained by the isoform-specific amino acid composition of the N-terminal α-helices, each of which bend into and constrict the funnel structure of the pore (12, 55). This proposition is in line with several gap junction mutagenesis studies demonstrating that the amino acid side chain charges in the N terminus are crucial for charge selectivity and thus ion conductance (56–62). In addition to the N-terminal pore-lining residues, the amino acids bordering TM1/E1 and in E1 are thought to be important for selective permeability and general gap junction and hemichannel properties (15, 39, 63–66), which coincides well with the observed DCFS-activated membrane current from oocytes expressing the E1 chimera ($Cx43^{30E1}$). The Cx43 C terminus is notably longer than that of Cx30, and truncation of the C terminus (Met-257) promotes Cx43 hemichannel-mediated conductance (30). Combination of C-terminal truncation with exchange of the N terminus and first extracellular loop with that of Cx30 generated a fully functional mutant Cx43 hemichannel capable of supporting Gd^{3+}-sensitive, DCFS-induced currents of a magnitude comparable with that of the Cx30 hemichannel. The ability of the Cx43 hemichannel to discriminate between atomic ions and ethidium in its open conformation appears to be determined by the N and C termini in combination with the first extracellular loop and thus not the actual membrane-spanning transmembrane domain 1. The ability to discriminate could in principle be explained by two gates in series (involving E1 and the N terminus/C terminus, respectively), where any voltage drop across a gate would close one gate but not the other (and vice versa). This type of contingent gating was demonstrated for gap junctional channels (67), and if gates were to flicker (as suggested by the temperature dependence of dye transfer through Cx43 hemichannels (30)), they would preclude an open conductive state while still allowing a concentration-driven shuttling of dye through the channel. Cx43 hemichannels have been proposed to be permeable to a variety of other molecules (*i.e.* prostaglandin E2, NAD^+, cAMP, ATP, and glutamate) (45–47, 68–70). Although it would be of interest to include ATP, and possibly other molecules, in a biophysical characterization such as the one employed in the present study, we have in our experimental system been unable to detect connexin-mediated DCFS-induced ATP release with the standard luciferase assay (35).

It is possible to at least partially rationalize these results using atomistic models of the connexin hemichannels, based on the known structures of Cx26 (see Ref. 12 for Cx30) and Cx46/Cx50 (see Ref. 41 for Cx43). This division was chosen to obtain the highest degree of similarity to each connexin. Notably, similar results were obtained with Cx26 as a base for the Cx43 atomistic model (data not shown). Charged residues lining the pore are responsible for important changes in the permeation pathways of ions, and this is especially true in the E1 region bordering TM1, where the channel is narrower and stiff (42). Cx30 and Cx43 display crucial differences in the number and position of acidic residues facing the pore in this region. In Cx26, which shares a high sequence similarity with Cx30, the amino acid residues Asp-50, Glu-47, Asp-46, and Glu-42 have been associated with the ability of the channel to coordinate calcium ions (42, 71). Moreover, a single amino acid substitution at position 50 (D50N, D50A, or D50C) impairs the ability of Cx26 (and Cx30 (35)) hemichannels to close correctly in response of high extracellular calcium concentration, while reducing the hemichannel conductance in the open state (39). The permeation pathways of the two hemichannels indeed reveal important differences in the region around the first extracellular loop: The Cx30 hemichannel can accumulate potassium ions with more ease, whereas the same region in Cx43 appears to be impermeable to monovalent atomic cations. In agreement with the experimental data, substitution of Cx43 extracellular loop 1

with that of Cx30 in the atomistic model produces a density profile in this very region that is comparable with Cx30 and suggests ion permeation in this chimeric model. Single point substitution of residues in the E1 part of the pore-lining region bordering the TM1 has no effect. Whereas the different energy barriers that regulate permeation within the channel act independently, the ability of ions or other molecules to pass through the channel is dictated by the possibility of passing each of such barriers. Therefore, single amino acid changes to the sequences of Cx43 are not sufficient to reproduce the higher conductance state of Cx30. Our simulations, on the other hand, did not show important differences in the potassium density at the level of the N-terminal helix. It is possible that another gating mechanism regulates the ion passage in this region of the channel, possibly involving conformational changes that are not detectable in the absence of C-terminal modeling (due to its flexibility and unstructured organization) or by the current state-of-the-art atomistic simulations (44, 72, 73).

The pharmacological tools within the connexin field are challenged by cross-reactivity between isoforms and other large pore channels and the lack of proven channel specificity (9–11, 75). As a further complication, connexin hemichannel inhibition depends on the permeant under investigation (this study and 29). The well-established gap junction and hemichannel blocker FFA (11, 75) displayed a connexin isoform-specific inhibitory potency with regard to ion conductance, whereas no inhibitory effect was observed on the hemichannel-mediated ethidium uptake. No such FFA permeant-dependent isoform-specific inhibition has been described previously, whereas fluorescent dye, ion conductance, ATP, and glutamate inhibition in astrocytes or C6 cells expressing Cx43 have been reported (22, 76, 77). La^{3+} displayed no isoform-specific inhibition but exhibited a permeant-dependent potency with a ~4 times lower ethidium IC_{50} compared with the IC_{50} for the atomic ions. This La^{3+} potency difference between ethidium and atomic ions is comparable with previously observed IC_{50} differences (ethidium *versus* atomic ions) in Cx30 exposed to either Ca^{2+} (~4.5-fold) or Mg^{2+} (~3.5-fold) (35). Surprisingly, the higher La^{3+} sensitivity observed for Cx30-mediated ethidium uptake *versus* ion conductance is the opposite of what we previously observed for gadolinium, which displayed higher potency toward the conductance pathways in Cx30 hemichannels than toward the ethidium uptake (29). The conventional Px1 inhibitors probenecid and CBX displayed different actions on the connexin hemichannels: Probenecid had no effect on the connexin hemichannel-mediated ethidium uptake, whereas it inhibited the ion conductance of both isoforms by ~25% when used at the concentrations normally employed in the pannexin research field (78, 79). In contrast, CBX displayed isoform-specific potency toward both permeants, as reported previously for dye uptake by different connexin isoforms exposed to CBX (29), with complete block of Cx26-mediated current at 100 μM. The fact that connexins and pannexins are expressed in many of the same cell types and share some activation mechanisms and permeants (1, 7, 9, 11) compromises the use of probenecid and, especially, CBX as tools to delineate pannexin function and thus calls for novel inhibitors that offer higher specificity. The mimetic peptide gap27, which is identical to part of the second extracellular loop of Cx43, had, as expected, no appreciable effect on Cx26/30 hemichannel-mediated ion conductance. However, we observed no inhibition of DCFS-induced ethidium uptake through either Cx30 or Cx43. Similarly, a recent report showed no Gap27 inhibitory effect on the Cx32-E143 hemichannel, whereas, on the other hand, attenuating Px1-mediated ion conductance (80). In contrast, other research groups have reported that gap27 blocks Cx43-mediated dye uptake (and ATP release) in cultured astrocytes and GP8 endothelial and HeLa cells (76, 81, 82). The action of the peptide may therefore rely on the experimental design, such as employed solutions and cell types, incubation time, manner of hemichannel activation, solvent, and other factors that may influence the mimetic peptide. According to the present data, FFA and CBX could be employed to experimentally distinguish between membrane currents arising from atomic ion permeation through Cx26 and Cx30 hemichannels while keeping in mind other "off target" channels present in native cells (11). Our results demonstrate that inhibition of fluorescent dye uptake does not necessarily reflect equal inhibition of current and that inhibition of fluorescent dye uptake therefore may not serve as an appropriate proxy for (patho)physiological connexin hemichannel activity.

In conclusion, our experimental data together with the computational data suggest that Cx43 in its hemichannel configuration does not act exactly as a half-gap junction in the sense that its gap junctional atomic ion conductance (83) is not reproduced in its hemichannel configuration. The structural determinants dictating the ability to allow hemichannel-mediated dye uptake while precluding atomic ion permeation reside in the outer parts of the pore-lining region: the N terminus and the first extracellular loop, in conjunction with the C terminus. These regions are similarly involved in channel selectivity and gating in the gap junction configuration of the connexins and appear to contribute the isoform-specific and selective connexin hemichannel permeability. Our results emphasize the notion that connexins do not form freely diffusible channels with simple size-based discrimination of their permeant(s) and that fluorescent dye transfer (or inhibition thereof) may not be an appropriate tool to determine biological connexin hemichannel activity in a given experimental setting.

Materials and methods

Mutagenesis and in vitro transcription

cDNA encoding mCx30 (from Klaus Willecke, Bonn University) or rCx43 (from Zealand Pharma, Denmark) was subcloned into the oocyte expression–optimized pXOOM expression vector (84) and verified by DNA sequencing (Eurofins Genomics). The QuikChange site-directed mutagenesis kit (Stratagene) was used to introduce point mutations into Cx43, verified by DNA sequencing. Cx30 and Cx43 chimeras were purchased through Genscript (Nanjing, China). All constructs were enzymatically linearized downstream from the poly(A) segment and *in vitro* transcribed into cRNA using the T7 mMessage Machine protocol (Ambion, Austin, TX). MEGAclear (Ambion) was used to extract the cRNA, which was stored at −80 °C prior to use.

Oocyte preparation

The surgical removal and preparation of the oocytes was done as described previously (85) under a license issued by the experimental animal inspectorate, the Danish Ministry of Justice, and in a accordance with the European Community guidelines for the use of experimental animals. Prior to cRNA injection, the oocytes were kept in Kulori medium: 90 mM NaCl, 1 mM KCl, 1 mM $MgCl_2$, 1 mM $CaCl_2$, 5 mM HEPES, adjusted to pH 7.4 with 2 M Tris-base ($(HOCH_2)_3CNH_2$)) for 24 h at 18 °C. After microinjection (10 ng of cRNA/oocyte), the oocytes were kept for 3–4 days at 18 °C in Kulori medium before used for experiments. No siRNA against the previously reported endogenous XeCx38 (50) was used, because uninjected control oocytes do not display any Ca^{2+}- or Gd^{3+}-sensitive conductance or dye uptake under our experimental conditions (11, 30).

Electrophysiology

Connexin-mediated conductance was measured by two-electrode voltage clamp at room temperature with borosilicate glass capillary electrodes pulled to a resistance of 1–4 megaohms when filled with 1 M KCl. A Dagan Clampator connected to a computer with a Digidata 1440 A/D converter and pClamp 9.2–10.4 (Axon Instruments, Molecular Devices, San Jose, CA) were used to obtain the measurements, and the current was low pass–filtered at 500 Hz and sampled at 2 kHz. *I*/V curves were derived from a 200-ms 11-step voltage clamp protocol (−140 to +60 mV) from a holding potential of −30 mV. The control solution contained 100 mM NaCl, 2 mM KCl, 1 mM $CaCl_2$, 1 mM $MgCl_2$, 10 mM HEPES, adjusted to pH 7.4 with 2 M Tris-base ($(HOCH_2)_3CNH_2$). The equiosmolar DCFS contained 103 mM NaCl, 2 mM KCl, 10 mM HEPES, adjusted to pH 7.4 with 2 M Tris-base ($(HOCH_2)_3CNH_2$).

Ethidium uptake

Oocytes (six per condition) were washed in the relevant test solution (see solution content above) before incubating and mildly aggregating them in a 24-well plate, each well containing 500 μl of the same test solution with 50 μM ethidium bromide for 40 min (ethidium uptake was linear within this time frame (87)). The oocytes were subsequently washed three times in control solution, individually transferred to a well in a 96-well plate, and lysed by repeated pipetting in 50 μl of ddH_2O. A Synergy HT plate reader (BioTek, Winooski, VT) with 360/40- and 590/35-nm filters and Gen5 software (BioTek) was used to measure the fluorescence intensity. For the inhibitor experiments, subtraction of background ethidium uptake in uninjected oocytes exposed to the same concentrations of inhibitor was performed to exclude nonspecific effects of the inhibitors and to obtain the connexin-specific response.

Surface biotinylation and Western blotting

Oocytes (10 of each expressing either WT Cx30, WT Cx43, chimeras of Cx30 and Cx43, or one of the Cx43 point mutations) were transferred to a 24-well plate, washed once in PBS-CM (PBS containing 1 mM $CaCl_2$ and 0.1 mM $MgCl_2$, pH 7.5) and once in biotinylation buffer (10 mM triethanolamine, 2 mM $CaCl_2$, and 125 mM NaCl, pH 8.9), prior to incubation for 45 min at 4 °C in ice-cold biotinylation buffer containing sulfo-NHS-SS-biotin (1.5 mg/ml final concentration; Thermo Scientific, Rockford, IL). Prior to cell lysis, sonication, and centrifugation, the oocytes were washed twice in ice-cold quenching buffer (50 mM Tris-HCl in PBS-CM, pH 8.0) and once in PBS-CM. The cleared lysates were transferred to spin columns containing Immobilized NeutrAvidin gel slurry (Thermo Scientific) and incubated for 1 h at room temperature in a tube rotator. After repeated washing, sample buffer (containing 7.5 mg/ml DTT) was added to the spin columns prior to an additional 1-h rotation at room temperature. The samples were centrifuged and analyzed by SDS-PAGE and Western blotting using anti-Cx43 (1:8000; C6219, Sigma/Merck KGaA, Darmstadt, Germany) followed by anti-rabbit secondary antibody (1:15,000; P/N 926-32211, LI-COR, Lincoln, NE).

Homology modeling and molecular dynamics simulation

The input sequence for the Cx43 homology models was amino acids 1–244 (UniprotKB-P17302). The Cx43 homology model employed for the sequence alignment and predicted pore-lining amino acids (Figs. 1 and 2) was generated using the Cx26 3.5 Å X-ray crystal (12). For the homology models used for molecular dynamics simulations in Fig. 6, the different levels of sequence similarity were taken into account. The chosen template structures were the Cx26 3.5 Å X-ray crystal (12) for the Cx30 model and the Cx46/Cx50 cryo-EM gap junction channel (41) for all of the other models. The molecular dynamics simulation followed the same protocol used for the Cx26 and Cx30 hemichannels (42). For the sake of internal consistency of the results presented in this paper, we did not use old results, but repeated the simulations also for Cx30. Starting configurations of Cx30, Cx43, and the chimera proteins were obtained by homology modeling using the Swiss-PDB webserver (88, 89). All of the models were truncated at the position homologous to amino acid 226 in Cx26. Each hemichannel model was then inserted in a phospholipid bilayer membrane, after performing an energy minimization protocol *in vacuo* aimed at eliminating bad contacts in the newly formed connexon. The systems were subsequently solvated with full atom TIP3P water, containing Cl^- and K^+ ions at a concentration of ~0.15 M to mimic a physiological ionic strength. With such inclusion of water and ions, each of the five atomistic models contained around 210,000 atoms. The systems underwent a second round of energy minimization, followed by a short (10-ns) molecular dynamics equilibration at constant volume and periodic boundary conditions. We then performed an equilibrium molecular dynamics simulation under periodic boundary conditions at constant pressure for an additional 250 ns. Simulations were performed using the Gromacs 2016 software package (90) and the Amber14ffSB force field for protein and membranes (91). Temperature (*T*) was kept fixed at 300 K in all simulations, and, where stated, the pressure (*P*) was fixed at 1 atm using a Berendsen thermostat and barostat (86). Fast smooth particle-mesh Ewald summation (74) was used for long-range electrostatic interactions, with a cutoff of 1.0 nm for the direct interactions. The K^+ and Cl^- densities were calculated using a script that tracked the amount of ions inside the channel along the molecular dynamics trajectory.

Chemicals

Ethidium bromide (50 μM) was from Sigma/Merck KGaA and was diluted from a liquid stock of 25 mM. $GdCl_3$ (Gd^{3+}, 100 mM stock in ddH_2O), FFA (100 mM stock in DMSO), La^{3+} (100 mM stock in ddH_2O), probenecid (100 mM stock in 100 mM NaOH), and CBX (100 mM stock in ddH_2O) were all from Sigma/Merck KGaA. The mimetic peptide gap27 (dissolved directly into the test solution) was kindly provided by Zealand Pharma (Glostrup, Denmark). In all cases, the relevant solvent vehicle was included in the experiment to ensure constant solvent concentrations.

Statistics and data analysis

All oocyte experiments were from at least three different frog donors. For the electrophysiological experiments, *n* equals the number of oocytes, and for ethidium uptake, *n* equals the number of experiments (each conducted with at least six oocytes). The equation, $Y = 100/(1 + 10\ ((\log IC_{50} - X) \times \text{Hill slope}))$, in GraphPad Prism 6–7 (GraphPad Software, Inc., La Jolla, CA) was used to fit the IC_{50} curves. The statistical analyses were performed with GraphPad Prism 6–7 and the tests indicated in the figure legends. Data represent the mean ± S.D., and $p < 0.05$ was considered statistically significant.

Author contributions—B. S. N., M. S. N., and N. M. conceptualization; B. S. N., F. Z., and M. S. N. formal analysis; B. S. N. and M. S. N. validation; B. S. N., F. Z., T. F., and T. L. investigation; B. S. N. and F. Z. visualization; B. S. N., F. Z., T. F., T. L., and N. M. methodology; B. S. N. and N. M. writing-original draft; B. S. N. and N. M. project administration; B. S. N., F. Z., T. F., T. L., M. S. N., and N. M. writing-review and editing; M. S. N. and N. M. supervision; N. M. data curation; N. M. funding acquisition.

References

1. Harris, A. L. (2007) Connexin channel permeability to cytoplasmic molecules. *Prog. Biophys. Mol. Biol.* **94,** 120–143 CrossRef Medline
2. Nielsen, M. S., Axelsen, L. N., Sorgen, P. L., Verma, V., Delmar, M., and Holstein-Rathlou, N. H. (2012) Gap junctions. *Compr. Physiol.* **2,** 1981–2035 CrossRef Medline
3. Söhl, G., and Willecke, K. (2003) An update on connexin genes and their nomenclature in mouse and man. *Cell Commun. Adhes.* **10,** 173–180 CrossRef Medline
4. Harris, A. L., and Locke, D. (2009) Permeability of connexin channels. in *Connexins: A Guide* (Harris, A. L., and Locke, D., eds) pp. 165–206, Humana Press, Totowa, NJ
5. Veenstra, R. D. (1996) Size and selectivity of gap junction channels formed from different connexins. *J. Bioenerg. Biomembr.* **28,** 327–337 CrossRef Medline
6. Hofer, A., and Dermietzel, R. (1998) Visualization and functional blocking of gap junction hemichannels (connexons) with antibodies against external loop domains in astrocytes. *Glia* **24,** 141–154 CrossRef Medline
7. Scemes, E., Spray, D. C., and Meda, P. (2009) Connexins, pannexins, innexins: novel roles of "hemi-channels". *Pflugers Arch.* **457,** 1207–1226 CrossRef Medline
8. Dahl, G. (2007) Gap junction-mimetic peptides do work, but in unexpected ways. *Cell Commun. Adhes.* **14,** 259–264 CrossRef Medline
9. Spray, D. C., Ye, Z. C., and Ransom, B. R. (2006) Functional connexin "hemichannels": a critical appraisal. *Glia* **54,** 758–773 CrossRef Medline
10. Ye, Z. C., Oberheim, N., Kettenmann, H., and Ransom, B. R. (2009) Pharmacological "cross-inhibition" of connexin hemichannels and swelling activated anion channels. *Glia* **57,** 258–269 CrossRef Medline
11. Nielsen, B. S., Hansen, D. B., Ransom, B. R., Nielsen, M. S., and MacAulay, N. (2017) Connexin hemichannels in astrocytes: an assessment of controversies regarding their functional characteristics. *Neurochem. Res.* **42,** 2537–2550 CrossRef Medline
12. Maeda, S., Nakagawa, S., Suga, M., Yamashita, E., Oshima, A., Fujiyoshi, Y., and Tsukihara, T. (2009) Structure of the connexin 26 gap junction channel at 3.5 Å resolution. *Nature* **458,** 597–602 CrossRef Medline
13. Hu, X., and Dahl, G. (1999) Exchange of conductance and gating properties between gap junction hemichannels. *FEBS Lett.* **451,** 113–117 CrossRef Medline
14. Hu, X., Ma, M., and Dahl, G. (2006) Conductance of connexin hemichannels segregates with the first transmembrane segment. *Biophys. J.* **90,** 140–150 CrossRef Medline
15. Kronengold, J., Trexler, E. B., Bukauskas, F. F., Bargiello, T. A., and Verselis, V. K. (2003) Single-channel SCAM identifies pore-lining residues in the first extracellular loop and first transmembrane domains of Cx46 hemichannels. *J. Gen. Physiol.* **122,** 389–405 CrossRef Medline
16. Ma, M., and Dahl, G. (2006) Cosegregation of permeability and single-channel conductance in chimeric connexins. *Biophys. J.* **90,** 151–163 CrossRef Medline
17. Skerrett, M., Kasperek, E., Cao, F. L., Shin, J. H., Aronowitz, J., Ahmed, S., and Nicholson, B. J. (2001) Application of SCAM (substituted cysteine accessibility method) to gap junction intercellular channels. *Cell Commun. Adhes.* **8,** 179–185 CrossRef Medline
18. Zhou, X. W., Pfahnl, A., Werner, R., Hudder, A., Llanes, A., Luebke, A., and Dahl, G. (1997) Identification of a pore lining segment in gap junction hemichannels. *Biophys. J.* **72,** 1946–1953 CrossRef Medline
19. Abbaci, M., Barberi-Heyob, M., Blondel, W., Guillemin, F., and Didelon, J. (2008) Advantages and limitations of commonly used methods to assay the molecular permeability of gap junctional intercellular communication. *BioTechniques* **45,** 33–52, 56–62 CrossRef Medline
20. Orellana, J. A., Díaz, E., Schalper, K. A., Vargas, A. A., Bennett, M. V., and Sáez, J. C. (2011) Cation permeation through connexin 43 hemichannels is cooperative, competitive and saturable with parameters depending on the permeant species. *Biochem. Biophys. Res. Commun.* **409,** 603–609 CrossRef Medline
21. Ramachandran, S., Xie, L. H., John, S. A., Subramaniam, S., and Lal, R. (2007) A novel role for connexin hemichannel in oxidative stress and smoking-induced cell injury. *PLoS One* **2,** e712 CrossRef Medline
22. Ye, Z. C., Wyeth, M. S., Baltan-Tekkok, S., and Ransom, B. R. (2003) Functional hemichannels in astrocytes: a novel mechanism of glutamate release. *J. Neurosci.* **23,** 3588–3596 CrossRef Medline
23. Sáez, J. C., Schalper, K. A., Retamal, M. A., Orellana, J. A., Shoji, K. F., and Bennett, M. V. (2010) Cell membrane permeabilization via connexin hemichannels in living and dying cells. *Exp. Cell Res.* **316,** 2377–2389 CrossRef Medline
24. Li, H., Liu, T. F., Lazrak, A., Peracchia, C., Goldberg, G. S., Lampe, P. D., and Johnson, R. G. (1996) Properties and regulation of gap junctional hemichannels in the plasma membranes of cultured cells. *J. Cell Biol.* **134,** 1019–1030 CrossRef Medline
25. Bahima, L., Aleu, J., Elias, M., Martín-Satué, M., Muhaisen, A., Blasi, J., Marsal, J., and Solsona, C. (2006) Endogenous hemichannels play a role in the release of ATP from *Xenopus* oocytes. *J. Cell Physiol.* **206,** 95–102 CrossRef Medline
26. Contreras, J. E., Sánchez, H. A., Eugenin, E. A., Speidel, D., Theis, M., Willecke, K., Bukauskas, F. F., Bennett, M. V., and Sáez, J. C. (2002) Metabolic inhibition induces opening of unapposed connexin 43 gap junction hemichannels and reduces gap junctional communication in cortical astrocytes in culture. *Proc. Natl. Acad. Sci. U.S.A.* **99,** 495–500 CrossRef Medline
27. John, S. A., Kondo, R., Wang, S. Y., Goldhaber, J. I., and Weiss, J. N. (1999) Connexin-43 hemichannels opened by metabolic inhibition. *J. Biol. Chem.* **274,** 236–240 CrossRef Medline
28. Weber, P. A., Chang, H. C., Spaeth, K. E., Nitsche, J. M., and Nicholson, B. J. (2004) The permeability of gap junction channels to probes of different size is dependent on connexin composition and permeant-pore affinities. *Biophys. J.* **87,** 958–973 CrossRef Medline

29. Hansen, D. B., Ye, Z. C., Calloe, K., Braunstein, T. H., Hofgaard, J. P., Ransom, B. R., Nielsen, M. S., and MacAulay, N. (2014) Activation, permeability, and inhibition of astrocytic and neuronal large pore (hemi-)channels. *J. Biol. Chem.* **289,** 26058–26073 CrossRef Medline
30. Hansen, D. B., Braunstein, T. H., Nielsen, M. S., and MacAulay, N. (2014) Distinct permeation profiles of the connexin 30 and 43 hemichannels. *FEBS Lett.* **588,** 1446–1457 CrossRef Medline
31. Berger, A. C., Kelly, J. J., Lajoie, P., Shao, Q., and Laird, D. W. (2014) Mutations in Cx30 that are linked to skin disease and non-syndromic hearing loss exhibit several distinct cellular pathologies. *J. Cell Sci.* **127,** 1751–1764 CrossRef Medline
32. Essenfelder, G. M., Bruzzone, R., Lamartine, J., Charollais, A., Blanchet-Bardon, C., Barbe, M. T., Meda, P., and Waksman, G. (2004) Connexin30 mutations responsible for hidrotic ectodermal dysplasia cause abnormal hemichannel activity. *Hum. Mol. Genet.* **13,** 1703–1714 CrossRef Medline
33. Lai, A., Le, D. N., Paznekas, W. A., Gifford, W. D., Jabs, E. W., and Charles, A. C. (2006) Oculodentodigital dysplasia connexin43 mutations result in non-functional connexin hemichannels and gap junctions in C6 glioma cells. *J. Cell Sci.* **119,** 532–541 CrossRef Medline
34. Lopez, W., Liu, Y., Harris, A. L., and Contreras, J. E. (2014) Divalent regulation and intersubunit interactions of human connexin26 (Cx26) hemichannels. *Channels* **8,** 1–4 CrossRef Medline
35. Nielsen, B. S., Alstrom, J. S., Nicholson, B. J., Nielsen, M. S., and MacAulay, N. (2017) Permeant-specific gating of connexin 30 hemichannels. *J. Biol. Chem.* **292,** 19999–20009 CrossRef Medline
36. Ripps, H., Qian, H., and Zakevicius, J. (2004) Properties of connexin26 hemichannels expressed in *Xenopus* oocytes. *Cell Mol. Neurobiol.* **24,** 647–665 CrossRef Medline
37. Roux, L., Madar, A., Lacroix, M. M., Yi, C., Benchenane, K., and Giaume, C. (2015) Astroglial connexin 43 hemichannels modulate olfactory bulb slow oscillations. *J. Neurosci.* **35,** 15339–15352 CrossRef Medline
38. Sanchez, H. A., and Verselis, V. K. (2014) Aberrant Cx26 hemichannels and keratitis-ichthyosis-deafness syndrome: insights into syndromic hearing loss. *Front. Cell Neurosci.* **8,** 354 CrossRef Medline
39. Sanchez, H. A., Villone, K., Srinivas, M., and Verselis, V. K. (2013) The D50N mutation and syndromic deafness: altered Cx26 hemichannel properties caused by effects on the pore and intersubunit interactions. *J. Gen. Physiol.* **142,** 3–22 CrossRef Medline
40. Valiunas, V., and Weingart, R. (2000) Electrical properties of gap junction hemichannels identified in transfected HeLa cells. *Pflugers Arch.* **440,** 366–379 CrossRef Medline
41. Myers, J. B., Haddad, B. G., O'Neill, S. E., Chorev, D. S., Yoshioka, C. C., Robinson, C. V., Zuckerman, D. M., and Reichow, S. L. (2018) Structure of native lens connexin 46/50 intercellular channels by cryo-EM. *Nature* **564,** 372–377 CrossRef Medline
42. Zonta, F., Buratto, D., Cassini, C., Bortolozzi, M., and Mammano, F. (2014) Molecular dynamics simulations highlight structural and functional alterations in deafness-related M34T mutation of connexin 26. *Front. Physiol.* **5,** 85 CrossRef Medline
43. Zonta, F., Polles, G., Zanotti, G., and Mammano, F. (2012) Permeation pathway of homomeric connexin 26 and connexin 30 channels investigated by molecular dynamics. *J. Biomol. Struct. Dyn.* **29,** 985–998 CrossRef Medline
44. Zonta, F., Buratto, D., Crispino, G., Carrer, A., Bruno, F., Yang, G., Mammano, F., and Pantano, S. (2018) Cues to opening mechanisms from *in silico* electric field excitation of Cx26 hemichannel and *in vitro* mutagenesis studies in HeLa transfectans. *Front. Mol. Neurosci.* **11,** 170 CrossRef Medline
45. Valiunas, V. (2013) Cyclic nucleotide permeability through unopposed connexin hemichannels. *Front. Pharmacol.* **4,** 75 CrossRef Medline
46. Contreras, J. E., Sáez, J. C., Bukauskas, F. F., and Bennett, M. V. (2003) Gating and regulation of connexin 43 (Cx43) hemichannels. *Proc. Natl. Acad. Sci. U.S.A.* **100,** 11388–11393 CrossRef Medline
47. Wang, N., De Bock, M., Antoons, G., Gadicherla, A. K., Bol, M., Decrock, E., Evans, W. H., Sipido, K. R., Bukauskas, F. F., and Leybaert, L. (2012) Connexin mimetic peptides inhibit Cx43 hemichannel opening triggered by voltage and intracellular Ca^{2+} elevation. *Basic Res. Cardiol.* **107,** 304 CrossRef Medline
48. Srinivas, M., Jannace, T. F., Cocozzelli, A. G., Li, L., Slavi, N., Sellitto, C., and White, T. W. (2019) Connexin43 mutations linked to skin disease have augmented hemichannel activity. *Sci. Rep.* **9,** 19 CrossRef Medline
49. Barrio, L. C., Suchyna, T., Bargiello, T., Xu, L. X., Roginski, R. S., Bennett, M. V., and Nicholson, B. J. (1991) Gap junctions formed by connexins 26 and 32 alone and in combination are differently affected by applied voltage. *Proc. Natl. Acad. Sci. U.S.A.* **88,** 8410–8414 CrossRef Medline
50. Ebihara, L. (1996) *Xenopus* connexin38 forms hemi-gap-junctional channels in the nonjunctional plasma membrane of *Xenopus* oocytes. *Biophys, J.* **71,** 742–748 CrossRef Medline
51. Bao, X., Altenberg, G. A., and Reuss, L. (2004) Mechanism of regulation of the gap junction protein connexin 43 by protein kinase C-mediated phosphorylation. *Am. J. Physiol. Cell Physiol.* **286,** C647–C654 CrossRef Medline
52. Figueroa, V. A., Retamal, M. A., Cea, L. A., Salas, J. D., Vargas, A. A., Verdugo, C. A., Jara, O., Martínez, A. D., and Sáez, J. C. (2014) Extracellular gentamicin reduces the activity of connexin hemichannels and interferes with purinergic Ca^{2+} signaling in HeLa cells. *Front. Cell Neurosci.* **8,** 265 CrossRef Medline
53. Dahl, G., Levine, E., Rabadan-Diehl, C., and Werner, R. (1991) Cell/cell channel formation involves disulfide exchange. *Eur. J. Biochem.* **197,** 141–144 CrossRef Medline
54. Retamal, M. A., García, I. E., Pinto, B. I., Pupo, A., Báez, D., Stehberg, J., Del Rio, R., and González, C. (2016) Extracellular cysteine in connexins: role as redox sensors. *Front. Physiol.* **7,** 1 Medline
55. Bennett, B. C., Purdy, M. D., Baker, K. A., Acharya, C., McIntire, W. E., Stevens, R. C., Zhang, Q., Harris, A. L., Abagyan, R., and Yeager, M. (2016) An electrostatic mechanism for Ca^{2+}-mediated regulation of gap junction channels. *Nat. Commun.* **7,** 8770 CrossRef Medline
56. Dong, L., Liu, X., Li, H., Vertel, B. M., and Ebihara, L. (2006) Role of the N-terminus in permeability of chicken connexin45.6 gap junctional channels. *J. Physiol.* **576,** 787–799 CrossRef Medline
57. Gemel, J., Lin, X., Veenstra, R. D., and Beyer, E. C. (2006) N-terminal residues in Cx43 and Cx40 determine physiological properties of gap junction channels, but do not influence heteromeric assembly with each other or with Cx26. *J. Cell Sci.* **119,** 2258–2268 CrossRef Medline
58. Kyle, J. W., Minogue, P. J., Thomas, B. C., Domowicz, D. A., Berthoud, V. M., Hanck, D. A., and Beyer, E. C. (2008) An intact connexin N-terminus is required for function but not gap junction formation. *J. Cell Sci.* **121,** 2744–2750 CrossRef Medline
59. Musa, H., Fenn, E., Crye, M., Gemel, J., Beyer, E. C., and Veenstra, R. D. (2004) Amino terminal glutamate residues confer spermine sensitivity and affect voltage gating and channel conductance of rat connexin40 gap junctions. *J. Physiol.* **557,** 863–878 CrossRef Medline
60. Oh, S., Verselis, V. K., and Bargiello, T. A. (2008) Charges dispersed over the permeation pathway determine the charge selectivity and conductance of a Cx32 chimeric hemichannel. *J. Physiol.* **586,** 2445–2461 CrossRef Medline
61. Xin, L., Gong, X. Q., and Bai, D. (2010) The role of amino terminus of mouse Cx50 in determining transjunctional voltage-dependent gating and unitary conductance. *Biophys. J.* **99,** 2077–2086 CrossRef Medline
62. Xin, L., Nakagawa, S., Tsukihara, T., and Bai, D. (2012) Aspartic acid residue D3 critically determines Cx50 gap junction channel transjunctional voltage-dependent gating and unitary conductance. *Biophys. J.* **102,** 1022–1031 CrossRef Medline
63. Tong, J. J., Minogue, P. J., Guo, W., Chen, T. L., Beyer, E. C., Berthoud, V. M., and Ebihara, L. (2011) Different consequences of cataract-associated mutations at adjacent positions in the first extracellular boundary of connexin50. *Am. J. Physiol. Cell Physiol.* **300,** C1055–C1064 CrossRef Medline
64. Tong, X., Aoyama, H., Sudhakar, S., Chen, H., Shilton, B. H., and Bai, D. (2015) The first extracellular domain plays an important role in unitary channel conductance of Cx50 gap junction channels. *PLoS One* **10,** e0143876 CrossRef Medline
65. Tong, X., Aoyama, H., Tsukihara, T., and Bai, D. (2014) Charge at the 46th residue of connexin 50 is crucial for the gap-junctional unitary conductance and transjunctional voltage-dependent gating. *J. Physiol.* **592,** 5187–5202 CrossRef Medline

66. Trexler, E. B., Bukauskas, F. F., Kronengold, J., Bargiello, T. A., and Verselis, V. K. (2000) The first extracellular loop domain is a major determinant of charge selectivity in connexin46 channels. *Biophys. J.* **79,** 3036–3051 CrossRef Medline
67. Harris, A. L., Spray, D. C., and Bennett, M. V. (1981) Kinetic properties of a voltage-dependent junctional conductance. *J. Gen. Physiol.* **77,** 95–117 CrossRef Medline
68. Bruzzone, S., Guida, L., Zocchi, E., Franco, L., and De Flora, A. (2001) Connexin 43 hemi channels mediate Ca^{2+}-regulated transmembrane NAD^+ fluxes in intact cells. *FASEB J.* **15,** 10–12 CrossRef Medline
69. Cherian, P. P., Siller-Jackson, A. J., Gu, S., Wang, X., Bonewald, L. F., Sprague, E., and Jiang, J. X. (2005) Mechanical strain opens connexin 43 hemichannels in osteocytes: a novel mechanism for the release of prostaglandin. *Mol. Biol. Cell* **16,** 3100–3106 CrossRef Medline
70. Kang, J., Kang, N., Lovatt, D., Torres, A., Zhao, Z., Lin, J., and Nedergaard, M. (2008) Connexin 43 hemichannels are permeable to ATP. *J. Neurosci.* **28,** 4702–4711 CrossRef Medline
71. Lopez, W., Ramachandran, J., Alsamarah, A., Luo, Y., Harris, A. L., and Contreras, J. E. (2016) Mechanism of gating by calcium in connexin hemichannels. *Proc. Natl. Acad. Sci. U.S.A.* **113,** E7986–E7995 CrossRef Medline
72. Bargiello, T. A., Oh, S., Tang, Q., Bargiello, N. K., Dowd, T. L., and Kwon, T. (2018) Gating of connexin channels by transjunctional-voltage: conformations and models of open and closed states. *Biochim. Biophys. Acta Biomembr.* **1860,** 22–39 CrossRef Medline
73. Verselis, V. K., Ginter, C. S., and Bargiello, T. A. (1994) Opposite voltage gating polarities of two closely related connexins. *Nature* **368,** 348–351 CrossRef Medline
74. Darden, T., York, D., and Pedersen, L. (1993) Particle mesh Ewald: an *N*.log(*N*) method for Ewald sums in large systems. *J. Chem. Phys.* **98,** 10089–10092 CrossRef
75. D'hondt, C., Ponsaerts, R., De Smedt, H., Bultynck, G., and Himpens, B. (2009) Pannexins, distant relatives of the connexin family with specific cellular functions? *Bioessays* **31,** 953–974 CrossRef Medline
76. Braet, K., Aspeslagh, S., Vandamme, W., Willecke, K., Martin, P. E., Evans, W. H., and Leybaert, L. (2003) Pharmacological sensitivity of ATP release triggered by photoliberation of inositol-1,4,5-trisphosphate and zero extracellular calcium in brain endothelial cells. *J. Cell Physiol.* **197,** 205–213 CrossRef Medline
77. Stout, C. E., Costantin, J. L., Naus, C. C., and Charles, A. C. (2002) Intercellular calcium signaling in astrocytes via ATP release through connexin hemichannels. *J. Biol. Chem.* **277,** 10482–10488 CrossRef Medline
78. Ma, W., Hui, H., Pelegrin, P., and Surprenant, A. (2009) Pharmacological characterization of pannexin-1 currents expressed in mammalian cells. *J. Pharmacol. Exp. Ther.* **328,** 409–418 CrossRef Medline
79. Silverman, W., Locovei, S., and Dahl, G. (2008) Probenecid, a gout remedy, inhibits pannexin 1 channels. *Am. J. Physiol. Cell Physiol.* **295,** C761–C767 CrossRef Medline
80. Wang, J., Ma, M., Locovei, S., Keane, R. W., and Dahl, G. (2007) Modulation of membrane channel currents by gap junction protein mimetic peptides: size matters. *Am. J. Physiol. Cell Physiol.* **293,** C1112–C1119 CrossRef Medline
81. Wei, H., Deng, F., Chen, Y., Qin, Y., Hao, Y., and Guo, X. (2014) Ultrafine carbon black induces glutamate and ATP release by activating connexin and pannexin hemichannels in cultured astrocytes. *Toxicology* **323,** 32–41 CrossRef Medline
82. Retamal, M. A., Froger, N., Palacios-Prado, N., Ezan, P., Sáez, P. J., Sáez, J. C., and Giaume, C. (2007) Cx43 hemichannels and gap junction channels in astrocytes are regulated oppositely by proinflammatory cytokines released from activated microglia. *J. Neurosci.* **27,** 13781–13792 CrossRef Medline
83. Wang, H. Z., and Veenstra, R. D. (1997) Monovalent ion selectivity sequences of the rat connexin43 gap junction channel. *J. Gen. Physiol.* **109,** 491–507 CrossRef Medline
84. Jespersen, T., Grunnet, M., Angelo, K., Klaerke, D. A., and Olesen, S. P. (2002) Dual-function vector for protein expression in both mammalian cells and *Xenopus laevis* oocytes. *BioTechniques* **32,** 536–538, 540 CrossRef Medline
85. Fenton, R. A., Moeller, H. B., Zelenina, M., Snaebjornsson, M. T., Holen, T., and MacAulay, N. (2010) Differential water permeability and regulation of three aquaporin 4 isoforms. *Cell Mol. Life Sci.* **67,** 829–840 CrossRef Medline
86. Berendsen, H. J. C., Postma, J. P. M., Vangunsteren, W. F., Dinola, A., and Haak, J. R. (1984) Molecular dynamics with coupling to an external bath. *J. Chem. Phys.* **81,** 3684–3690 CrossRef
87. Alstrøm, J. S., Hansen, D. B., Nielsen, M. S., and MacAulay, N. (2015) Isoform-specific phosphorylation-dependent regulation of connexin hemichannels. *J. Neurophysiol.* **114,** 3014–3022 CrossRef Medline
88. Biasini, M., Bienert, S., Waterhouse, A., Arnold, K., Studer, G., Schmidt, T., Kiefer, F., Gallo Cassarino, T., Bertoni, M., Bordoli, L., and Schwede, T. (2014) SWISS-MODEL: modelling protein tertiary and quaternary structure using evolutionary information. *Nucleic Acids Res.* **42,** W252–W258 CrossRef Medline
89. Waterhouse, A., Bertoni, M., Bienert, S., Studer, G., Tauriello, G., Gumienny, R., Heer, F. T., de Beer, T. A. P., Rempfer, C., Bordoli, L., Lepore, R., and Schwede, T. (2018) SWISS-MODEL: homology modelling of protein structures and complexes. *Nucleic Acids Res.* **46,** W296–W303 CrossRef Medline
90. Pronk, S., Páll, S., Schulz, R., Larsson, P., Bjelkmar, P., Apostolov, R., Shirts, M. R., Smith, J. C., Kasson, P. M., van der Spoel, D., Hess, B., and Lindahl, E. (2013) GROMACS 4.5: a high-throughput and highly parallel open source molecular simulation toolkit. *Bioinformatics* **29,** 845–854 CrossRef Medline
91. Lindorff-Larsen, K., Piana, S., Palmo, K., Maragakis, P., Klepeis, J. L., Dror, R. O., and Shaw, D. E. (2010) Improved side-chain torsion potentials for the Amber ff99SB protein force field. *Proteins* **78,** 1950–1958 CrossRef Medline

Structural determinants underlying permeant discrimination of the Cx43 hemichannel

Brian Skriver Nielsen, Francesco Zonta, Thomas Farkas, Thomas Litman, Morten Schak Nielsen and Nanna MacAulay

J. Biol. Chem. 2019, 294:16789-16803.
doi: 10.1074/jbc.RA119.007732 originally published online September 25, 2019